UDC 621.313 https://doi.org/10.20998/2074-272X.2024.3.10

G. Boudechiche, O. Aissa, M. Sarra, I. Griche

Solar shunt active power filter based on optimized direct power control strategy with disturbance rejection principle

Introduction. *This paper focuses on a renewable energy system coupled to a dual purpose power grid via a parallel active power filter for injecting photovoltaic energy into the grid and improving the power quality in the presence of the non-linear load.* ***The novelty*** *of the work consists in the combination of two advanced techniques – Fuzzy Logic Controller (FLC) and the optimized Anti-Windup Fractional Order Proportional-Integral Differentiator (AW-FOPID) regulator based on Particle Swarm Optimization with the Spreading Factor (PSO-SF) algorithm, applied to the improved Direct Power Control (DPC) strategy under different conditions related to climate changes and healthy or infected electrical network.* ***Purpose.*** *Its main role is to improve the power quality and reject the perturbations deforming the electrical network under distorted, unbalanced and balanced grid voltage conditions. Besides, the FLC is employed the Maximum Power Point Tracking (MPPT) under any weather conditions. In addition, the optimized AW-FOPID controller leads to keep the DC bus voltage at its reference value with small undershoots and overshoots in the voltage with a short response time in steady or dynamic states.* ***Methods****. The rejection of disturbances affecting the grid is offered by the improved DPC. On the other hand, an intelligent method based on fuzzy logic was used MPPT under any weather conditions. Furthermore, an AW-FOPID regulator based on PSO-SF algorithm is used to keep the DC bus voltage at its reference value with small undershoots and overshoots in the voltage, while keeping a fast response time.* ***Results.*** *The proposed system control is evaluated in various states of power source: distorted, unbalanced, and balanced by simulation using MATLAB/Simulink. The simulation results illustrate the effectiveness and performance of the studied control strategies.* References 26, tables 8, figures 16.

Key words: **improved direct power control, particle swarm optimization, disturbance rejection principle, fuzzy maximum power point tracking.**

Вступ. *У цій статті основна увага приділяється системі відновлюваної енергії, що з'єднана з енергосистемою подвійного призначення через паралельний фільтр активної потужності для подачі фотоелектричної енергії в мережу та покращення якості електроенергії за наявності нелінійного навантаження.* ***Новизна*** *роботи полягає у поєднанні двох передових методик – Fuzzy Logic Controller (FLC) та оптимізованого регулятора Anti-Windup Fractional Order Proportional-Integral Differentiator (AW-FOPID) на основі оптимізації рою частинок з коефіцієнтом розширення (PSO-SF), що застосовується до покращеної стратегії прямого управління потужністю (DPC) у різних умовах, пов'язаних зі змінами клімату та справною або зараженою електричною мережею.* ***Мета***. *Його основна роль полягає в покращенні якості електроенергії та усуненні збурень, що деформують електричну мережу в умовах спотвореної, незбалансованої та збалансованої напруги мережі. Крім того, у FLC використовується система відстеження точки максимальної потужності (MPPT) за будь-яких погодних умов. Крім того, оптимізований контролер AW-FOPID дозволяє підтримувати напругу шини постійного струму на опорному значенні з невеликими відхиленнями і викидами напруги з коротким часом відгуку в стані динамічного стану.* ***Методи***. *Відмова від перешкод, що впливають на мережу, забезпечує покращений DPC. З іншого боку, інтелектуальний метод, заснований на нечіткій логіці, використовувався MPPT за будь-яких погодних умов. Крім того, регулятор AW-FOPID, заснований на алгоритмі PSO-SF, використовується для підтримки опорного значення напруги постійного струму шини з невеликими відхиленнями і викидами напруги, зберігаючи при цьому малий час відгуку.* ***Результати***. *Пропоноване управління системою оцінюється у різних станах джерела живлення: спотвореному, незбалансованому та збалансованому шляхом моделювання з використанням MATLAB/Simulink. Результати моделювання ілюструють ефективність та продуктивність вивчених стратегій управління.* Бібл. 26, табл. 8, рис. 16.

Ключові слова: **покращене пряме керування потужністю, оптимізація рою частинок, принцип придушення перешкод, нечітке відстеження точки максимальної потужності.**

1. Introduction. Energy production is a major concern in the future because it is considered one of the engines of sustainability of development projects [1]. Currently, fossil fuels provide the majority of the world's energy (gas, oil, and coal). Excessive use of non-renewable energy depletes reserves of this type of energy and contributes to greenhouse gas emissions, which pollute the environment and deadly threat to organisms [2]. Solar energy's availability is as an environmentally friendly, limitless, and free power source on the entire glob's surface [3]. Meanwhile, the growing usage of non-linear loads in the residential sector, and industrial sectors, causes problems related to the quality of energy [4]. These devices act as generators of harmonic currents inducing a consumption of reactive power [5]. To remedy these disadvantages, a curative solution consists in connecting a filtering device composing of an inverter in parallel with the system: nonlinear load – three-phase power source [6]. This Shunt Active Power Filter (SAPF) injects a current that opposes the reactive power and current harmonics emitted by the nonlinear load, to eventually makes the source current sinusoidal and in phase with its voltage, is frequently used [7, 8]. In the literature, many commands schemes have been adopted to control the SAPF. Hysteresis current approach is one of the most known methods [9]. However, it operates with a variable switching frequency [6]. To overcome such problem, authors have been suggested other commands such as Direct Power Control (DPC) [10, 11]. This command does not need Pulse-Width Modulation (PWM) or current control loops [12]. DPC is represented by a reference to the active power and another reference of the zero reactive power [13]. Nevertheless, these methods present also some issues related to high sampling rate and variable switching frequency [5]. To remedy these disadvantages, it is important to introduce other DPC structures. These later are represented in the DPC with space vector modulation which is used a linear Proportional Integral (PI) controllers and modulator of voltage instead of a hysteresis comparators and switching table [14]. However, this method requires the use of setting of the PI regulators and

coordinate transforms. For this reason, researchers, suggest other technique that known as predictive DPC, characterized by high accuracy [15]. Although this method needs complex calculations [9]. Nevertheless, when the aforementioned commands are used in distorted or unbalanced conditions of the power source, the performance of the system is deteriorated with degradation of the Total Harmonic Distortion (THD) contents which appears in input currents.

Goal of the article. This paper presents a new DPC method in order to improve the power quality under distorted, unbalanced or balanced grid voltage conditions. Moreover, this command needs to have zero disturbance references in reactive and active power.

Various regulators are used to keep the DC-link voltage at its desired value. Among them, the traditional PI regulator, which offers an excellent responsiveness in steady state [16], but performs poorly in transient states [11]. To remedy this problem, the suggested regulator in this paper is performed by an Anti-Windup Fractional Order Proportional-Integral Differentiator AW-FO($PI^{\varepsilon}D^{\eta}$) regulator, replacing the traditional PI regulator that maintains the DC-link voltage at its reference value. This AW-FO($PI^{\varepsilon}D^{\eta}$) regulator with two extra freedom degrees ε and η presents shorter response time and better dynamic response compared to the traditional PI regulator [17, 18]. In contrast to the traditional PI regulator used in DPC, which has poor responses in dynamic conditions, the output of the AW-FOPID regulator contributes to the delivery of the active power. Concerning the setting of the AW-FOPID parameters, Particle Swarm Optimization (PSO) technique is used to minimize the objective function. In fact, this is the first time that the optimized AW-FOPID regulator has been integrated into the new DPC configuration.

As the irradiation varies, several techniques of Maximum Power Point Tracking (MPPT) have been proposed [19, 20]. In our research, Fuzzy Logic Controller (FLC) has been used to track the MPPT and to solve the problem of the rapidly changing irradiance [9]. This work proposes a combination of two advanced techniques, the optimized AW-FOPID and FLC, applied to the Improved DPC (IDPC) strategy under different conditions related to climate changes and healthy or infected electrical network.

2. Description of solar SAPF controlled by the IDPC with optimized AW-FOPID regulator based on PSO-SF algorithm.

2.1. Description of IDPC strategy for the SAPF. The rejection of disturbances affecting the grid is provided by the IDPC command. Its principle role consists to eliminate the unwanted harmonics of the source currents due to contamination and unbalance of the power in the presence of the photovoltaic (PV) system. The IDPC approach needs no reactive and active power perturbation reference to reject the influence of the deformed electrical network as shown in Fig. 1 [21]. The currents participating to the calculation of reactive and active powers are assessed as follows:

$$\begin{bmatrix} \xi I_{sa} \\ \xi I_{sb} \\ \xi I_{sc} \end{bmatrix} = \begin{bmatrix} I_{sa} \\ I_{sb} \\ I_{sc} \end{bmatrix} - \begin{bmatrix} I_{sa}^{*} \\ I_{sb}^{*} \\ I_{sc}^{*} \end{bmatrix}. \quad (1)$$

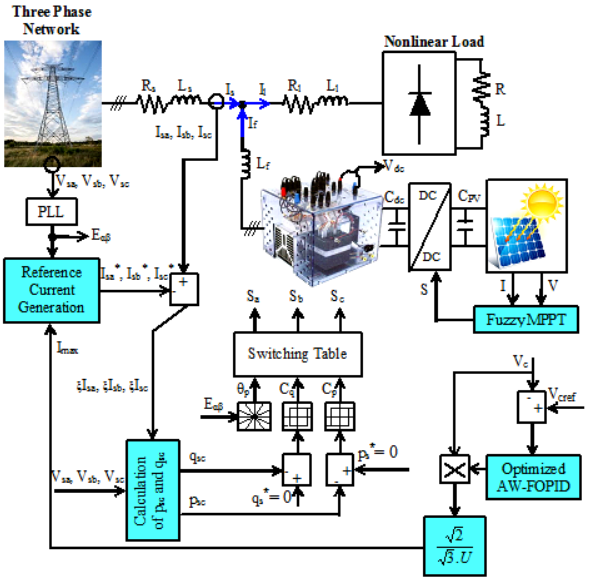

Fig. 1. SAPF articulated on the IDPC method with PV system

In the IDPC, the amplitude of the input currents I_{max} is given by the multiplication of the output voltage regulator AW-FOPID by the measured V_c voltage. This first result obtained is multiplied by a value gain $\sqrt{2}/\sqrt{3}U$. So, fundamental terms of these currents are delivered from the phase-locked loop block. The three reference source currents can be formulated as:

$$\begin{bmatrix} I_{sa}^{*} \\ I_{sb}^{*} \\ I_{sc}^{*} \end{bmatrix} = \begin{bmatrix} I_{\max}\sin(\omega t) \\ I_{\max}\sin(\omega t - 2\pi/3) \\ I_{\max}\sin(\omega t + 2\pi/3) \end{bmatrix}. \quad (2)$$

Substitution (2) in (1) gives the following equation:

$$\begin{bmatrix} \xi I_{sa} \\ \xi I_{sb} \\ \xi I_{sc} \end{bmatrix} = \begin{bmatrix} I_{sa} \\ I_{sb} \\ I_{sc} \end{bmatrix} - \begin{bmatrix} I_{\max}\sin(\omega t) \\ I_{\max}\sin(\omega t - 2\pi/3) \\ I_{\max}\sin(\omega t + 2\pi/3) \end{bmatrix}. \quad (3)$$

Consequently, instantaneous reactive and active powers (Q_{sc} and P_{sc}) provided by the harmonic component:

$$Q_{sc} = \frac{1}{\sqrt{3}}\left[(V_{sb} - V_{sc})\xi I_{sa} + (V_{sc} - V_{sa})\xi I_{sb} + (V_{sa} - V_{sb})\xi I_{sc}\right]; \quad (4)$$

$$P_{sc} = V_{sa}\xi I_{sa} + V_{sb}\xi I_{sb} + V_{sc}\xi I_{sc}, \quad (5)$$

where I_{sa}, I_{sb}, I_{sc}, V_{sa}, V_{sb}, V_{sc} are the distorted or unbalanced source currents and voltages of the phase A, B, C.

In this IDPC controller, the references of the active and reactive powers are set to zero value to ensure rejection of grid disturbances which are emitted by the load and to achieve a sinusoidal input current. For this reason, both reference active (psc^{*}) and reference reactive (qsc^{*}) powers and are set to zero.

2.2. AW-FOPID regulator based on PSO with the spreading factor (PSO-SF) algorithm.

Optimized AW-FOPID regulator. The traditional PI regulator suffers from some problem in the transient states [16]. To remedy this issue, the proposed regulator is performed by AW-FO($PI^{\varepsilon}D^{\eta}$), replacing the traditional PI regulator to keep the DC bus voltage at its reference value with small undershoots and overshoots in the voltage. The AW-FO$PI^{\varepsilon}D^{\eta}$ has a general form that includes the derivative η and the integral ε actions order, which are not integers

(Fig. 2). From Fig. 2, the transfer function of the optimized AW-FOPID regulator is given:

$$G(s)=\frac{U(s)}{E(s)}=K_p+K_i s^{-\varepsilon}+K_d s^{\eta}, \quad (6)$$

where K_d, K_p, K_i are the derivative, proportional and integral gain factors, respectively; η, ε are the derivative and integral orders respectively; $Y(s)$ is the output signal; $R(s)$ is the input signal, $E(s)$ is the error; $C(s)$ is the plant's transfer function. It is obvious that the choice of η and ε gives the traditional regulators, i.e. PI regulator (η = 0) and PID regulator (ε, η = 1).

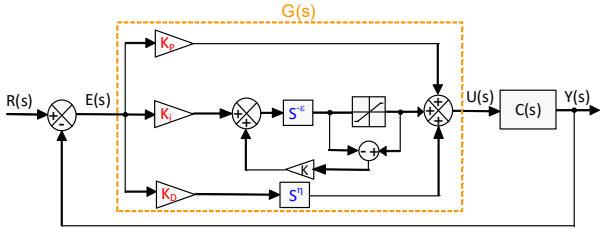

Fig. 2. General form regulator

a) Fractional Order Method. The technique suggested by Oustaloup in 1995 [17] adequate to approximate the Fractional Order (FO) to Laplace transfer functions. The Oustaloup's approximation model's term s^{β} is valid in the range [–1; 1]. s^{β} as an FO integrator if $\beta\in[-1; 0]$ and as an FO differentiator if $\beta\in[0; 1]$. In addition, this approximation employs a recursive distribution of zeroes and poles. So, the Oustaloup's approximation is evaluated as:

$$s^{\beta}=K\prod_{k=-M}^{M}\frac{s+\omega_k'}{s+\omega_k}, \quad (7)$$

where:

$$K=\omega_h^{\beta}, \quad (8)$$

$$\omega_k=\omega_b\left(\frac{\omega_h}{\omega_b}\right)^{\left(\frac{k+M+0.5(1+\beta)}{2M+1}\right)}, \quad (9)$$

$$\omega_k'=\omega_b\left(\frac{\omega_h}{\omega_b}\right)^{\left(\frac{k+M+0.5(1-\beta)}{2M+1}\right)}, \quad (10)$$

where ω_h, ω_b are the high and low frequencies, respectively; K is the adjustment gain; M is the number of zeros and poles; ω_k and ω_k' are respectively the poles and zeros of interval k; $(2M+1)$ is the approximation function order.

b) PSO with the Spreading Factor (PSO-SF). Depending on (6), the optimized AW-FOPID regulator has 5 parameters to be tuned (K_d, K_i, K_p, η, ε). Therefore, the PSO technique is used to tune the AW-FOPID parameters by minimizing the objective function f. PSO is a stochastic optimization algorithm based on the behaviour of swarms such as birds and fish [22-24]. In PSO technique, particle is regarded a potential solution for determining the best solution to the problem. Moreover, the position of a particle is influenced by its own best found position. The best position of the particle i is given as:

$$y_i(t+1)=\begin{cases}y_i(t) & \text{if} \quad f(x_i(t+1))\ge f(y_i(t)),\\ x_i(t+1) & \text{if} \quad f(x_i(t+1))< f(y_i(t)),\end{cases} \quad (11)$$

where f is the objective function; x_i is the particle's current position which is updated at time step t.

The basic PSO equations can be represented as:

$$x_i(t+1)=x_i(t)+V_i(t+1), \quad (12)$$

$$v_{i,j}=\omega\cdot v_{i,j}(t)+c_1\cdot\Delta_1+c_2\cdot\Delta_2, \quad (13)$$

where:

$$\Delta_1=r_{1,j}\cdot\left(y_{i,j}(t)-x_{i,j}(t)\right); \quad (14)$$

$$\Delta_2=r_{2,j}\cdot\left(y_j^n(t)-x_{i,j}(t)\right), \quad (15)$$

where c_1, c_2 are the acceleration constants, $v_{i,j}$ is the j^{th} element of the velocity vector of the i^{th} particle; $r_{1,j}$, $r_{2,j}$ are the random coefficients; ω is the inertia weight. This operation is stopped when the velocity updates tend to zero.

In PSO algorithm, each particle must update its own best individual objective function in each iteration. The individual objective function of each particle is calculated by using the integral time absolute error (MSE – Mean Squared Error):

$$MSE=\sum_{t_s=0}^{N}e^2\Big/N, \quad (16)$$

where t_s is the time rang of simulation; N is the total number of points for which the optimization is carried out; e is the error signal.

In this work, PSO with the spreading factor (PSO-SF) [25] is used instead of standard PSO to set the AW-FOPID regulator parameters. By applying the PSO-SF technique, the acceleration coefficient (c_1 and c_2) and inertia weight (ω) are given:

$$c_1=c_2=2\cdot(1-(\text{current epoch}/\text{total epoch})); \quad (17)$$

$$\omega=e^{(-\text{current epoch}/(SF\times\text{total epoch}))}; \quad (18)$$

where SF = 0.5(spread + deviation).

The algorithm's instructions to be followed of the tuning this regulator by PSO-SF:

1. Initialize the parameters of the 5 controller parameters: position range varies from 0.01 to 15; inertia weight ω from 0 to 1; velocity range varies from –0.001 to 0.5; acceleration c_1 and c_2 from 0.01 to 2;
2. Distribute particles at random within predefined ranges;
3. Evaluate the objective function by using (16) with MSE tending to 0;
4. Update new individual fitness if the present individual fitness is better to the prior individual fitness;
5. Identify the best particle objective function among the swarm;
6. Update the new population fitness if the present population fitness is better than the prior population fitness;
7. Use (12), (13) to determine the velocity and update the position;
8. Use (17), (18) to determine the new acceleration coefficients c_1 and c_2 and the inertia weight ω;
9. End.

2.3. Fuzzy MPPT. FLC is employed for tracking the MPP of PV array under any weather conditions [3]. This algorithm is very efficient for both nonlinear and linear systems [26]. The FLC has 3 steps: fuzzification, defuzzification and rules inference. The inputs of fuzzy MPPT are usually represented by a change in error ΔE and an error E [9]:

$$\begin{cases} E(k) = \Delta P / \Delta V; \\ \Delta E(k) = E(k) - E(k-1), \end{cases} \quad (19)$$

where:

$$\Delta V = V(k) - V(k-1); \quad (20)$$

$$\Delta P = P(k) - P(k-1); \quad (21)$$

where $V(k-1)$, $V(k)$, $P(k-1)$, $P(k)$ are respectively the voltage and the power of the PV at the sampling times $(k-1)$ and k [9].

The input variables $\Delta E(k)$ and $E(k)$ of fuzzy MPPT are divided into 5 fuzzy sets: Negative Small (*NS*), Positive Big (*PB*), Positive Small (*PS*), Zero (ZO) and Negative Big (*NB*). The rule base connects the fuzzy inputs to the fuzzy output by the syntax: «if *L* and *M*, then *N*» [9] (Table 1).

Table 1

Fuzzy MPPT

$\downarrow E/\Delta E \rightarrow$	*NB*	*NS*	*ZO*	*PS*	*PB*
NB	*PS*	*PB*	*PB*	*NB*	*NS*
NS	*ZO*	*PS*	*PS*	*NS*	*ZO*
ZO	*ZO*	*ZO*	*ZO*	*ZO*	*ZO*
PS	*ZO*	*NS*	*NS*	*PS*	*ZO*
PB	*NS*	*NB*	*NB*	*PB*	*PS*

The incremental duty cycle ΔD is calculated as [9]:

$$\Delta D = \sum_{j=0}^{n} w_j \Delta D_j \Big/ \sum_{j=0}^{n} w_j , \quad (22)$$

where ΔD_i is the value corresponding to ΔD; w is the weighting factor; n is the maximum number of effective rules.

Finally, the duty cycle is calculated by adding this modification to the control's prior value:

$$D(k+1) = D(k) + \Delta D(k). \quad (23)$$

3. Presentation and discussion of results. To validate the performance and feasibility of the approaches suggested in this paper, several simulation tests were run in the MATLAB/Simulink. Table 2 lists the parameters that were used for these tests.

Table 2

Parameters for the simulation

Parameter	Value	Parameter	Value
L_s, mH	0.1	L_l, mH	0.566
R_s, Ω	0.1	R_l, Ω	0.01
Switching frequency (DC/AC converter), kHz	20	Switching frequency (DC/DC boost converter), kHz	5
V_s, V	70	V_{cref}, V	227.68
f_s, Hz	50	C_{pv}, µF	20
L, mH	10	L_{pv}, mH	3
R, Ω	40	K_i	60
L_f, mH	2.5	K_d	0.011
R_f, Ω	0.01	K_p	0.95
C_{dc}, µF	2200	N	2
η	0.5	ε	0.4

Figure 3 illustrates the relationship between the current I and power P generated by the PV generator in response to different solar irradiation profiles G. Initially, prior to time t = 0.5 s, no power or current is produced when the solar irradiation is at zero. Subsequently, from 0.5 s to 2 s, the PV's power and current follow specific trajectories determined by the irradiation profile. During this period, the irradiation gradually rises from 0 to 800 W/m^2 until t = 0.9 s, resulting in the generation of 30 A with 4 kW output by using the FLC. At t = 0.9 s, the solar irradiation decreases from 800 to 300 W/m^2, leading to a decline in current from 30 A to 10 A and power from 4 kW to 1.43 kW. Then, at t = 1.3 s, the solar irradiation increases again, reaching 1000 W/m^2 and maintaining this level, thereby providing 5 kW with 40 A output.

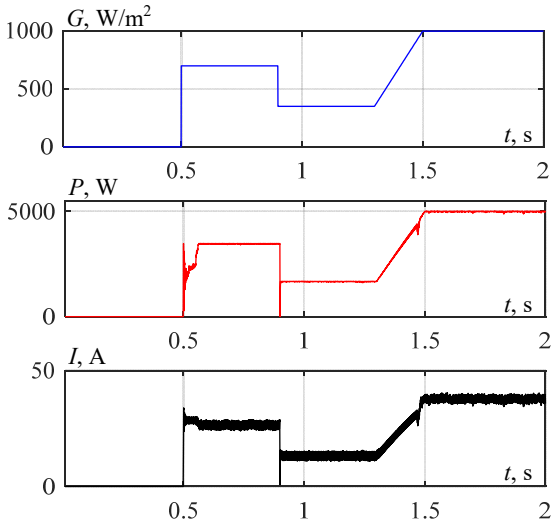

Fig. 3. Irradiation profile, power and current of the PV module

Figure 4 illustrates powers evolutions, obtained by the IDPC with optimized AW-FOPID and FLC MPPT. When the solar irradiation G = 0, the grid supplies the power P_s to the non-linear load P_l. Subsequently, upon the integration of the PV system, during the time interval [0.5, 2] s, the PV generator caters to the load's power demand P_f, with any excess power being fed back into the electrical network. From 0.1 to 2 s, the grid's reactive power Q_s is reduced to zero following the installation of the SAPF.

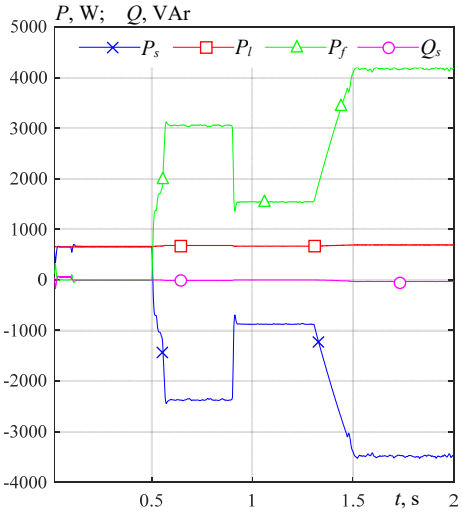

Fig. 4. Powers evolution for the proposed DPC

Figures 5, 7 display the current I_s and voltage V_s waveforms of the source, load current I_l and filter current I_f before and after filtering with and without the PV module.

In the absence of filtering and without PV integration, the source current exhibits distortion and deformation, with a THD of 30.35 %. However, upon the insertion of the SAPF at t = 0.1 s, the source current transforms into a sinusoidal waveform and synchronizes with the network voltage. Consequently, the THD is significantly reduced to 3.33 % for the IDPC with optimized AW-FOPID and 1.68 % for the IDPC with PI control (Table 3). Subsequently, during the period from

0.5 s to 2 s, SAPF comes into operation, ensuring that the source currents remain sinusoidal and in opposite phase to their corresponding voltages. As a result, the THD further decreases to 2.47 % for the IDPC with optimized AW-FOPID and 1.57 % for the IDPC with PI control (Table 3).

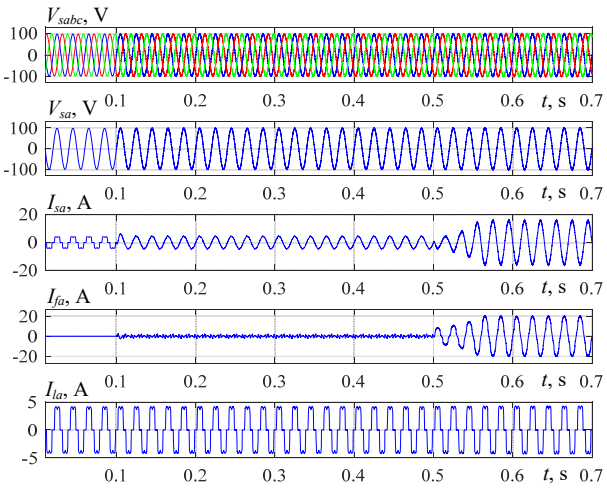

Fig. 5. Zoomed-in view on the SAPF articulated on IDPC with FLC and optimized AW-FOPID regulator: source currents and voltages, load and filter currents

Table 3
Comparison of source current THD for balanced network voltage

Control	Source current THD, %		
	Without SAPF	SAPF without PV	SAPF with PV
IDPC approach with optimized AW-FOPID regulator	30.35	3.33	2.47
IDPC approach with standard PI regulator	30.35	01.68	1.57

The DC-link voltage V_c stabilizes at its reference value V_{cref} during the introduction of the SAPF, and at each change in irradiation it returns to V_{cref}, justified by the exchange of energy between the nonlinear load, the grid, and the SAPF as shown in Fig. 6, 8 and Table 4.

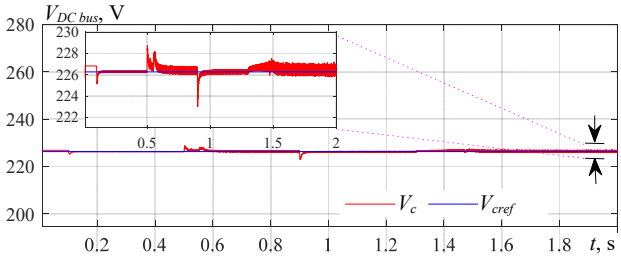

Fig. 6. Zoom on DC-link voltage of the SAPF articulated on IDPC with FLC and optimized AW-FOPID regulator

During the period [0.1, 0.5] s, where G = 0, it can be seen that V_c decreases from 226.27 V to 225.12 V for optimized AW-FOPID and 159.99 V for PI with response time 0.0182 s and 0.13 s, respectively. When G = 800 W/m^2 during [0.5-0.9] s, it can be noticed that V_c increases from 226.27 V to 229.26 V for optimized AW-FOPID and 265.7 V for PI with response time 0.077 s and 0.19 s, respectively. When G = 300 W/m^2 during the period [0.9-1.3] s, it can be observed that V_c decreases from 226.27 V to 221.99 V for optimized AW-FOPID and 193.68 V for PI with response time 0.047 s and 0.12 s, respectively. Finally, in the period [1.3-2] s, where G = 1000 W/m^2, it can be seen that V_c increases from 226.27 V to 227.3 V for optimized AW-FOPID and 237.5 V for PI with response time 0.174 s and 0.29 s, respectively.

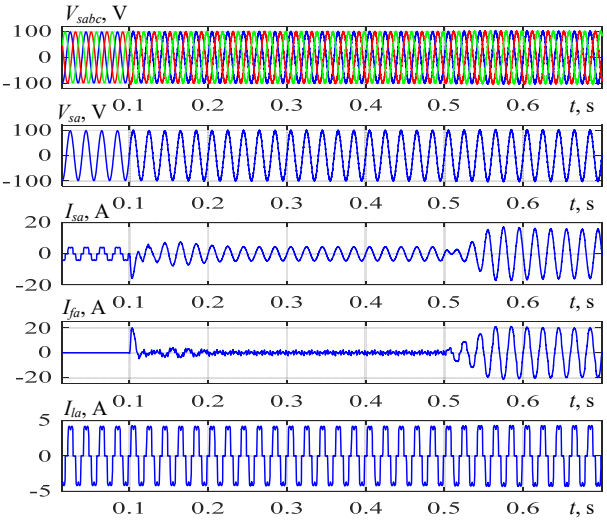

Fig. 7. Zoom of SAPF articulated on IDPC with FLC and PI regulator: source currents and voltages, load and filter currents

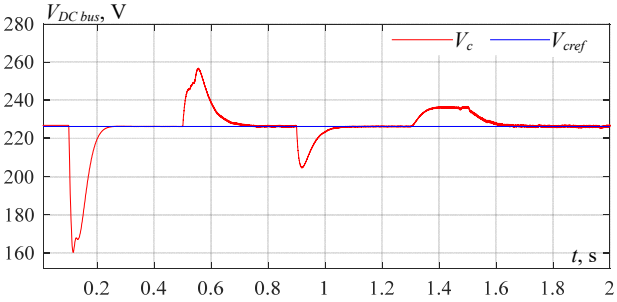

Fig. 8. Zoom on DC-link voltage of the SAPF articulated on IDPC equipped with FLC and PI regulator

Table 4
Comparison of the optimized AW-FOPID with traditional PI regulator under **balanced** network voltage and variations in solar irradiation

Control	IDPC approach with optimized AW-FOPID regulator	IDPC approach with PI regulator
SAPF without PV ΔV, V	Voltage drop of 1.15	Voltage drop of 66.28
SAPF without PV Δt, s	0.0182	0.13
SAPF with PV ΔV, V	Overshoot of 2.99	Overshoot of 39.43
	Voltage drop of 4.28	Voltage drop of 32.59
	Overshoot of 1.03	Overshoot of 11.23
SAPF with PV Δt, s	0.077	0.19
	0.047	0.12
	0.174	0.29

The optimized AW-FOPID regulator demonstrates notable advantages over the traditional PI regulator under balanced network voltage and varying solar irradiation conditions. Figures 6, 8 and Table 4 present the performance comparison, highlighting the following key aspects:

- *Voltage drops*. The optimized AW-FOPID regulator exhibits reduced voltage drops compared to the traditional PI regulator. This means that the AW-FOPID controller maintains a more stable voltage profile, minimizing fluctuations and ensuring a smoother operation.

• *Voltage overshoots*. The optimized AW-FOPID regulator also shows smaller voltage overshoots than the traditional PI regulator. This implies that the AW-FOPID controller achieves better control over the system's response, preventing excessive deviations and maintaining tighter regulation.

• *Short response time*. The optimized AW-FOPID regulator achieves a shorter response time compared to the traditional PI regulator. This indicates that the AW-FOPID controller can rapidly adapt to changes in the system, providing quicker and more accurate adjustments.

In summary, the optimized AW-FOPID regulator outperforms the traditional PI regulator in terms of voltage stability, response speed, and overall system control, making it a more efficient and effective choice for systems operating under balanced network voltage and varying solar irradiation conditions.

Unbalanced and distorted network voltages tests. A first test based on unbalanced network voltages is performed to test the robustness of the IDPC: V_{sa} = 70 V, V_{sb} = 120 V, V_{sc} = 60 V. The simulation results of the SAPF articulated on IDPC equipped with the optimized AW-FOPID, PI regulator and FLC, operating under unbalanced network voltage, are shown in Fig. 9, 11.

Figures 9, 11 display the source currents and voltages, the load currents and filter currents, after and before filtering, with and without PV array under unbalanced network voltages. Before filtering and without PV, the source current is deformed with THD is 30.32 %. After the SAPF is inserted at the instant 0.1 s, the source current becomes sinusoidal and synchronizes with network voltage. The THD in this situation is 3.76 % for the IDPC with optimized AW-FOPID and 3.21 % for the IDPC with PI (Table 5). Then from 0.5 to 2 s, the SAPF starts operating, where the source currents stay sinusoidal and in opposition phase with the corresponding voltages. So, THD is 4.57 % for the IDPC with optimized AW-FOPID and 3.8 % for the IDPC with PI (Table 5).

Table 5

Comparison of source current THD for unbalanced network voltage

Control	THD of source current, %	
	IDPC approach with optimized AW-FOPID regulator	IDPC approach with standard PI regulator
Without SAPF	30.32	30.32
SAPF without PV	3.76	3.21
SAPF with PV	4.57	3.8

During the period [0.1, 0.5] s, where G = 0, it can be seen that V_c increases from 226.27 V to 242.16 V for optimized AW-FOPID with response time 7.65 ms. The simulation results of the solar SAPF articulated on the IDPC equipped with the optimized AW-FOPID, PI regulator and FLC controller, operating under unbalanced network voltage, are shown in Fig. 9, 11. Whereas, it can be observed that V_c decreases from 226.27 V to 225.06 V for optimized AW-FOPID and 169.89 V for PI with response time 8 ms and 0.109 s, respectively. However, when G = 800W/m^2 during [0.5-0.9] s, it can be noticed that V_c increases from 226.27 V to 229.79 V for optimized AW-FOPID and 275.1 V for PI with response time 22.5 ms and 0.155 s, respectively.

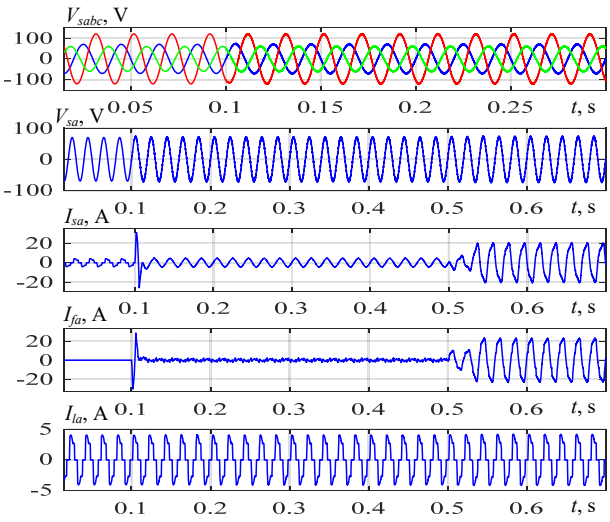

Fig. 9. Zoom of SAPF articulated on the IDPC with FLC and optimized AW-FOPID regulator under unbalanced network voltages: source currents and voltages, load and filter currents

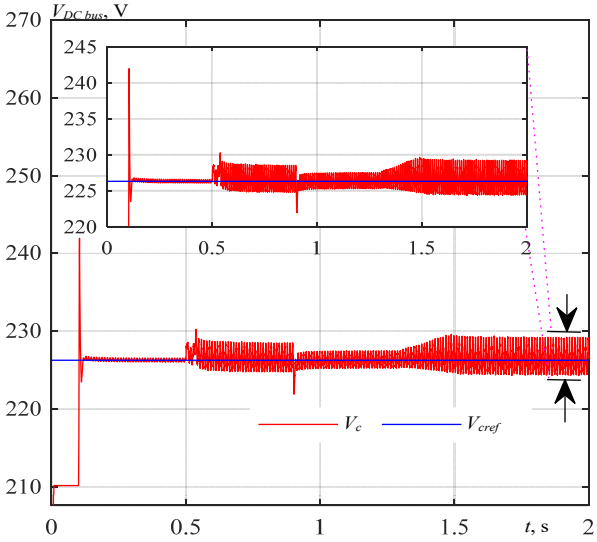

Fig. 10. Zoom on DC-link voltage of the SAPF articulated on the IDPC with FLC and optimized AW-PID regulator under unbalanced network voltages

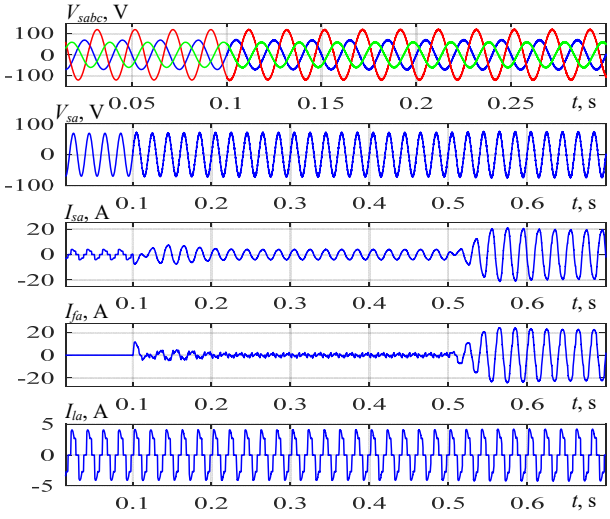

Fig. 11. Zoomed of SAPF articulated on the IDPC with FLC and PI regulator under unbalanced network voltages: source currents and voltages, load and filter currents

During the insertion of the SAPF, the DC-link voltage V_c stabilizes at its reference value V_{cref}. Additionally, at each

change in solar irradiation, the DC-link voltage returns to the reference value V_{cref} (Fig. 10, 12, Table 6). Then, when $G = 300$ W/m^2 during the period [0.9-1.3] s, it can be observed that V_c decreases from 226.27 V to 220.54 V for optimized AW-FOPID and 188 V for PI with response time 16.93 ms and 0.12 s, respectively. Finally, in the period [1.3-2] s, where $G = 1000$ W/m², it can be seen that V_c increases from 226.27 V to 246.81 V for PI with response time 0.7 s.

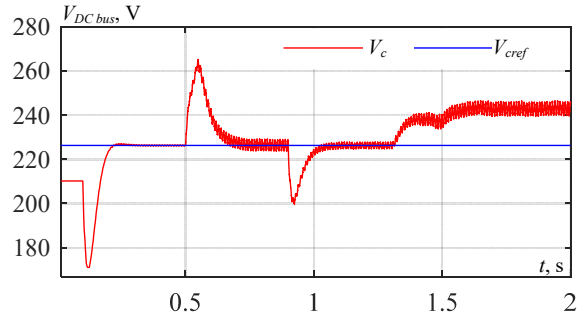

Fig. 12. Zoom on DC-link voltage of the SAPF articulated on the IDPC equipped with FLC and PI regulator under unbalanced network voltages

Table 6

Comparison of the optimized AW-FOPID with traditional PI regulator under **unbalanced** network voltage and variations in solar irradiation

Control	IDPC approach with optimized AW-FOPID regulator	IDPC approach with PI regulator
SAPF without PV ΔV, V	Overshoot of 15.89 Voltage drop of 1.21	Voltage drop of 56.38
SAPF without PV Δt, s	0.00765 0.008	0.109
SAPF with PV ΔV, V	Overshoot of 3.52 Voltage drop of 5.73	Overshoot of 48.83 Voltage drop of 38.27 Overshoot of 20.54
SAPF with PV Δt, s	0.0225 0.01693	0.155 0.12 0.7

In summary, the optimized AW-FOPID controller demonstrates better performance in maintaining the DC-link voltage V_c closer to its reference value V_{cref} during varying solar irradiation. It achieves faster response times and smaller voltage deviations compared to the traditional PI controller in most situations.

As a result, the optimized AW-FOPID regulator has a smaller voltage drops and overshoots with a short response time under unbalanced network voltage with variations in solar irradiation compared to those obtained from the traditional PI controller (Fig. 10, 12, Table 6).

The second test of the IDPC approach's robustness is articulated on network voltage distortion. In this test, the fundamental input voltages are superimposed with the fifth harmonic voltage. The simulation results of the solar SAPF articulated on the IDPC equipped with the optimized AW-FOPID, PI regulator and FLC controller, operating under distorted network voltage (Fig. 13, 15).

Figures 13, 15 present the waveforms of source currents and voltages, load currents, and filter currents before and after filtering, with and without the PV array under distorted network conditions. Initially, the source current is distorted and deformed with a THD of 36.9 %.

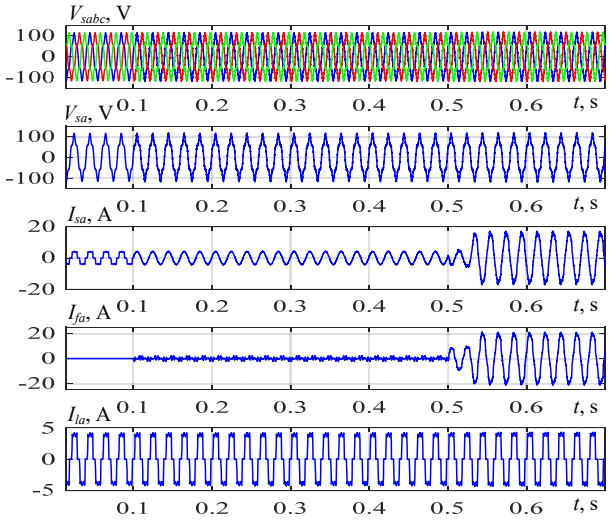

Fig. 13. Zoom of SAPF articulated on IDPC with FLC and optimized AW-PID regulator under distorted network voltages: source currents and voltages, load and filter currents

Upon the insertion of the SAPF at $t = 0.1$ s, the source current undergoes significant improvement, transforming into a sinusoidal waveform and synchronizing with the network voltage. The THD reduces to 2.97 % for the IDPC with optimized AW-FOPID and 3.02 % for the IDPC with PI control (Table 7).

Subsequently, from 0.5 s to 2 s, the SAPF becomes operational, resulting in the source currents remaining sinusoidal and in opposition phase to their corresponding voltages. During this period, the THD is 4.62 % for the IDPC with optimized AW-FOPID and 3.15 % for the IDPC with PI control (Table 7).

During the introduction of the SAPF, the DC-link voltage V_c stabilizes at its designated value V_{cref}, and whenever there is a change in solar irradiation, it returns to this reference value (Fig. 14, 16, Table 8).

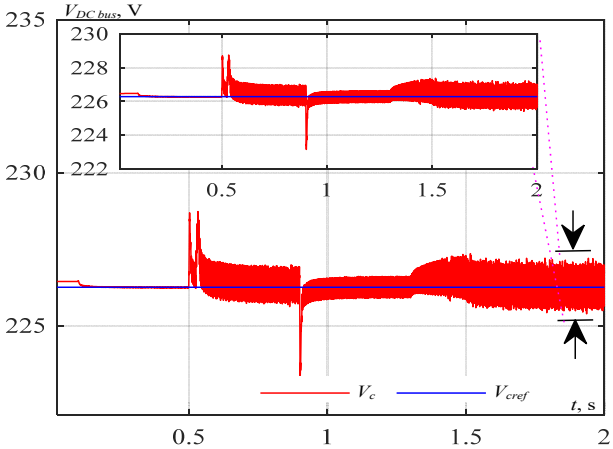

Fig. 14. Zoom on DC-link voltage of the SAPF articulated on the IDPC equipped with FLC and optimized AW-PID regulator under distorted network voltages

Table 7

Comparison of source current THD under distorted network voltage with variations in solar irradiation

Control	THD of source current, %	
	IDPC approach with optimized AW-FOPID regulator	IDPC approach with standard PI regulator
Without SAPF	36.9	36.9
SAPF without PV	2.97	3.02
SAPF with PV	4.62	3.15

Table 8

Comparison of the optimized AW-FOPID with classical PI under distorted grid voltage with variations in solar irradiation

Control	IDPC approach with optimized AW-FOPID regulator	IDPC approach with PI regulator
SAPF without PV ΔV, V	Overshoot of 1.64	Voltage drop of 69.27
SAPF without PV Δt, s	0.1	0.13
SAPF with PV ΔV, V	Overshoot of 3.29 Voltage drop of 4.28	Overshoot of 40.73 Voltage drop of 32.28 Overshoot of 12.23
SAPF with PV Δt, s	0.052 0.0296	0.18 0.15 0.313

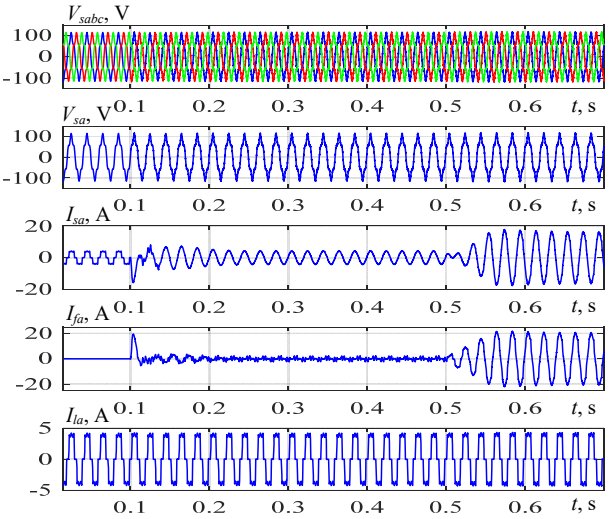

Fig. 15. Zoom of SAPF articulated on IDPC with FLC and PI regulator under distorted network voltages: source currents and voltages, load and filter currents

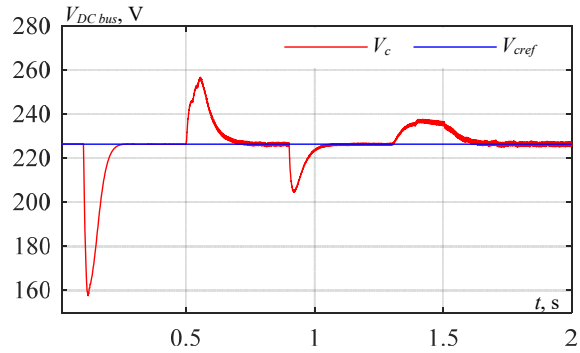

Fig. 16. Zoom on DC-link voltage of the SAPF articulated on the IDPC equipped with FLC and PI regulator under distorted network voltages

Let's summarize the observations during different periods:

• **Period [0.1, 0.5] s (G = 0).**

Optimized AW-FOPID: V_c increases from 226.27 V to 227.91 V with a response time 0.1 s.

PI: V_c decreases from 226.27 V to 157 V with a response time 0.13 s.

• **Period [0.5, 0.9] s (G = 800 W/m²):**

Optimized AW-FOPID: V_c increases from 226.27 V to 229.56 V with a response time 0.052 s.

PI: V_c increases from 226.27 V to 267 V with a response time 0.18 s.

• **Period [0.9, 1.3] s (G = 300 W/m²):**

Optimized AW-FOPID: V_c decreases from 226.27 V to 221.99 V with a response time 0.0296 s.

PI: V_c decreases from 226.27 V to 193.99 V with a response time 0.15 s.

• **Period [1.3, 2] s (G = 1000 W/m²):**

PI: V_c increases from 226.2 V to 238.5 V with a response time 0.313 s.

In summary, the DC-link voltage V_c in the system remains stable at the reference value V_{cref} during SAPF insertion and readjusts to this value at every change in solar irradiation. The optimized AW-FOPID regulator successfully maintains V_c close to its reference value with faster response times with fewer and smaller voltage deviations in most situations compared to the traditional PI regulator. However, during G = 1000 W/m², the PI regulator exhibits a higher response time and a slightly higher V_c value compared to the optimized AW-FOPID regulator. As a result, the optimized AW-FOPID regulator has a smaller voltage drops and overshoots with a short response time under distorted network voltage with variations in solar irradiation compared to those obtained from the traditional PI controller, as represented in Fig. 14, 16 and Table 8.

4. Conclusions. This paper investigates an improved Direct Power Control (DPC) articulated on optimized Anti-Windup Fractional Order Proportional-Integral Differentiator (AW-FOPID) regulator for a double-stage grid-interconnected photovoltaic system, associated with a Shunt Active Power Filter (SAPF). The primary objective is to reject the perturbations deforming the electrical network and ensures agreeable total harmonic distortion under distorted, unbalanced and balanced grid voltage conditions. The particle swarm optimization algorithm is employed to tune the parameters of the AW-FOPID regulator by minimizing an objective function. Therefore, the improved DPC strategy ensures efficient delivery of SAPF by replacing the traditional PI controller with the optimized AW-FOPID regulator. Moreover, a fuzzy logic controller is integrated into the system to effectively track the maximum power point under diverse weather conditions. The study's results demonstrate the superior performance of studied control strategies in terms of response time, undershoots and overshoot in the DC link voltage under distorted, unbalanced and balanced network voltage with variations in solar irradiation compared to those obtained from the traditional PI regulator.

Conflict of interest. The authors declare no conflict of interest.

REFERENCES

1. Mansouri N., Lashab A., Guerrero J.M., Cherif A. Photovoltaic power plants in electrical distribution networks: a review on their impact and solutions. *IET Renewable Power Generation*, 2020, vol. 14, no. 12, pp. 2114-2125. https://doi.org/10.1049/iet-rpg.2019.1172.

2. Lashab A., Sera D., Hahn F., Juarez Camurca L., Liserre M., Guerrero J.M. A Reduced Power Switches Count Multilevel Converter-Based Photovoltaic System With Integrated Energy Storage. *IEEE Transactions on Industrial Electronics*, 2021, vol. 68, no. 9, pp. 8231-8240. doi: https://doi.org/10.1109/TIE.2020.3009594.

3. Abouadane H., Fakkar A., Sera D., Lashab A., Spataru S., Kerekes T. Multiple-Power-Sample Based P&O MPPT for Fast-Changing Irradiance Conditions for a Simple Implementation. *IEEE Journal of Photovoltaics*, 2020, vol. 10, no. 5, pp. 1481-1488. doi: https://doi.org/10.1109/JPHOTOV.2020.3009781.

4. Youcefa B., Massoum A., Barkat S., Wira P. Backstepping Direct Power Control for Power Quality Enhancement of Grid-connected Photovoltaic System Implemented with PIL Co-simulation Technique. *Advances in Modelling and Analysis C*, 2019, vol. 74, no. 1, pp. 1-14. doi: https://doi.org/10.18280/ama_c.740101.
5. El Ouanjli N., Motahhir S., Derouich A., El Ghzizal A., Chebabhi A., Taoussi M. Improved DTC strategy of doubly fed induction motor using fuzzy logic controller. *Energy Reports*, 2019, vol. 5, pp. 271-279. doi: https://doi.org/10.1016/j.egyr.2019.02.001.
6. Aissa O., Moulahoum S., Colak I., Babes B., Kabache N. Analysis and experimental evaluation of shunt active power filter for power quality improvement based on predictive direct power control. *Environmental Science and Pollution Research*, 2018, vol. 25, no. 25), pp. 24548-24560. doi: https://doi.org/10.1007/s11356-017-0396-1.
7. Bourouis B., Djeghloud H., Benalla H. Energy efficiency of a 3-level shunt active power filter powered by a fuel-cell / battery DC bus with regulated duty cycles. *Electrical Engineering & Electromechanics*, 2021, no. 5, pp. 30-38. doi: https://doi.org/10.20998/2074-272X.2021.5.05.
8. Chemidi A., Benhabib M.C., Bourouis M.A. Performance improvement of shunt active power filter based on indirect control with a new robust phase-locked loop. *Electrical Engineering & Electromechanics*, 2022, no. 4, pp. 51-56. doi: https://doi.org/10.20998/2074-272X.2022.4.07.
9. Boudechiche G., Sarra M., Aissa O., Lashab A. Intelligent Solar Shunt Active Power Filter Based on Direct Power Control Strategy. *Lecture Notes in Networks and Systems*, 2021, vol. 174, pp. 467-477. doi: https://doi.org/10.1007/978-3-030-63846-7_44.
10. Noguchi T., Tomiki H., Kondo S., Takahashi I. Direct power control of PWM converter without power-source voltage sensors. *IEEE Transactions on Industry Applications*, 1998, vol. 34, no. 3, pp. 473-479. doi: https://doi.org/10.1109/28.673716.
11. Sarra M., Belkaid A., Colak I., Boudechiche G., Kayisli K. Fuzzy-MPPT Controller Based Solar Shunt Active Power Filter. *2022 11th International Conference on Renewable Energy Research and Application (ICRERA)*, 2022, pp. 436-440. doi: https://doi.org/10.1109/ICRERA55966.2022.9922873.
12. Essoussi B., Moutabir A., Bensassi B., Ouchatti A., Zahraoui Y., Benazza B. Power Quality Improvement using a New DPC Switching Table for a Three-Phase SAPF. *International Journal of Robotics and Control Systems*, 2023, vol. 3, no. 3, pp. 510-529. doi: https://doi.org/10.31763/ijrcs.v3i3.1042.
13. Naamane D., Laid Z., Fateh M. Power Quality Improvement Based on Third-Order Sliding Mode Direct Power Control of Microgrid-Connected Photovoltaic System with Battery Storage and Nonlinear Load. *Iranian Journal of Science and Technology, Transactions of Electrical Engineering*, 2023, vol. 47, no. 4, pp. 1473-1490. doi: https://doi.org/10.1007/s40998-023-00627-4.
14. Liu X., Qiu L., Wu W., Ma J., Fang Y., Peng Z., Wang D. Efficient model-free predictive power control for active front-end modular multilevel converter. *International Journal of Electrical Power & Energy Systems*, 2021, vol. 132, art. no. 107058. doi: https://doi.org/10.1016/j.ijepes.2021.107058.
15. Lhachemi H., Prieur C., Trelat E. PI Regulation of a Reaction–Diffusion Equation With Delayed Boundary Control. *IEEE Transactions on Automatic Control*, 2021, vol. 66, no. 4, pp. 1573-1587. doi: *https://doi.org/10.1109/TAC.2020.2996598*.
16. Boudechiche G., Sarra M., Aissa O., Gaubert J.-P., Benlahbib B., Lashab A. Anti-Windup FOPID-Based DPC for SAPF Interconnected to a PV System Tuned Using PSO Algorithm. *European Journal of Electrical Engineering*, 2020, vol. 22, no. 4-5, pp. 313-324. doi: https://doi.org/10.18280/ejee.224-503.
17. Oustaloup A. *La dérivation non entière: théorie, synthèse et applications*. Paris, 1995. 508 p. (Fra).
18. Oustaloup A., Levron F., Mathieu B., Nanot F.M. Frequency-band complex noninteger differentiator: characterization and synthesis. *IEEE Transactions on Circuits and Systems I: Fundamental Theory and Applications*, 2000, vol. 47, no. 1, pp. 25-39. doi: https://doi.org/10.1109/81.817385.
19. Zerzouri N., Ben Si Ali N., Benalia N. A maximum power point tracking of a photovoltaic system connected to a three-phase grid using a variable step size perturb and observe algorithm. *Electrical Engineering & Electromechanics*, 2023, no. 5, pp. 37-46. doi: https://doi.org/10.20998/2074-272X.2023.5.06.
20. Louarem S., Kebbab F.Z., Salhi H., Nouri H. A comparative study of maximum power point tracking techniques for a photovoltaic grid-connected system. *Electrical Engineering & Electromechanics*, 2022, no. 4, pp. 27-33. doi: https://doi.org/10.20998/2074-272X.2022.4.04.
21. Bouafia A., Gaubert J.P., Chaoui A. Direct power control scheme based on disturbance rejection principle for three-phase PWM AC/DC converter under different input voltage conditions. *Journal of Electrical Systems*, 2012, vol. 8, no. 4, pp. 367-383.
22. Abdelkader B., Merabti A., Yamina B. Using PSO algorithm for power flow management enhancement in PV-battery grid systems. *International Journal of Power Electronics and Drive Systems (IJPEDS)*, 2023, vol. 14, no. 1, pp. 413-425. doi: https://doi.org/10.11591/ijpeds.v14.i1.pp413-425.
23. Kennedy J., Eberhart R. *Particle swarm optimization*. *Proceedings of ICNN'95 - International Conference on Neural Networks*, 1995, vol. 4, pp. 1942-1948. doi: https://doi.org/10.1109/ICNN.1995.488968.
24. Benslimane A., Benslimane Y. Increase Stability and Efficiency in PV-Battery-Grid Systems Using PSO Algorithm. *European Journal of Electrical Engineering*, 2022, vol. 24, no. 2, pp. 113-121. doi: https://doi.org/10.18280/ejee.240206.
25. Abd Latiff I., Tokhi M.O. Fast convergence strategy for Particle Swarm Optimization using spread factor. *2009 IEEE Congress on Evolutionary Computation*, 2009, pp. 2693-2700. doi: https://doi.org/10.1109/CEC.2009.4983280.
26. Leopoldino A.L.M., Freitas C.M., Monteiro L.F.C.Analysis of the Hybrid PSO-InC MPPT for Different Partial Shading Conditions. *Advances in Electrical and Computer Engineering*, 2022, vol. 22, no. 2, pp. 29-36. doi: https://doi.org/10.4316/AECE.2022.02004.

Received 19.10.2023
Accepted 15.12.2023
Published 01.05.2024

Ghania Boudechiche[1], *Doctor of Engineering,*
Oualid Aissa[2], *Associate Professor,*
Mustapha Sarra[1], *Full Professor*,
Issam Griche[3], *Associate Professor,*
[1] ETA Laboratory, Electronics Department,
University Mohamed El-Bachir El-Ibrahimi of Bordj Bou Arreridj, Algeria,
e-mail: ghania.boudechiche@univ-bba.dz (Corresponding Author); mustapha.sarra@univ-bba.dz
[2] LPMRN Laboratory, Faculty of Sciences and Technology,
University Mohamed El-Bachir El-Ibrahimi of Bordj Bou Arreridj, Algeria,
e-mail: oualid.aissa@univ-bba.dz
[3] Department of Electrical Engineering,
University of Bouira, Algeria,
e-mail: griche_issam@yahoo.fr

How to cite this article:
Boudechiche G., Aissa O., Sarra M., Griche I. Solar shunt active power filter based on optimized direct power control strategy with disturbance rejection principle. *Electrical Engineering & Electromechanics*, 2024, no. 3, pp. 72-80. doi: https://doi.org/10.20998/2074-272X.2024.3.10